symmetry

Article

Observation of Hidden Asymmetry in Polarization Space for Dissipative Soliton Fiber Lasers

Yu Long , Qiang Wu , Zhenghu Chang, Ai Liu, Yuanjie Yu, Shiyun Dai, Peng Cai, Ligang Huang, Lei Gao * and Tao Zhu

Key Laboratory of Optoelectronic Technology & Systems (Ministry of Education), Chongqing University, Chongqing 400044, China
* Correspondence: gaolei@cqu.edu.cn; Tel.: +86-023-6511-1975

Abstract: Dissipative solitons appear widely in physical systems with dissipative energy exchange, which have been regarded as an excellent platform for exploring nonlinear dynamics. The complex interactions among dispersion management and nonlinearity result in abundant asymmetric behaviors in diverse parameter spaces. Nevertheless, conventional detection methods impede direct and single-shot measurements of the transient polarization dynamics of dissipative solitons. Here, by using the division-of-amplitude method combined with dispersive Fourier transform techniques, we have experimentally observed the internal evolution of dissipative solitons in polarization space. By disturbing the cavity birefringence, we obtain asymmetrical spectra due to nonlinear phase evolution within numerous temporal roundtrips. The different phases across the lasing wavelengths result in wavelength-resolved symmetric breakage in polarization space, which is difficult to find in spectrum or pulse-shape measurements. The direct observation of hidden asymmetry in polarization space for dissipative soliton fiber lasers will facilitate theoretical modeling of mode-locked laser systems with complicated configurations, and it may also promote applications for polarization spectroscopy.

Keywords: dissipative solitons; polarization; ultrafast fiber laser; phase; symmetry

Citation: Long, Y.; Wu, Q.; Chang, Z.; Liu, A.; Yu, Y.; Dai, S.; Cai, P.; Huang, L.; Gao, L.; Zhu, T. Observation of Hidden Asymmetry in Polarization Space for Dissipative Soliton Fiber Lasers. *Symmetry* **2023**, *15*, 95. https://doi.org/10.3390/sym15010095

Academic Editor: Luis L. Sánchez-Soto

Received: 26 November 2022
Revised: 23 December 2022
Accepted: 28 December 2022
Published: 29 December 2022

1. Introduction

Compared with the Hamiltonian system, a dissipative system has the dissipative property of continuously exchanging energy with the environment, which makes their behavior more complex [1]. Dissipative solitons (DSs) are a kind of soliton wave supported in dissipative systems with nonlinear gain or loss. They have been extensively studied in nonlinear physical fields, such as fluid mechanics, and photonics [2,3]. Passively mode-locked fiber lasers with dispersion management have been shown to be dissipative nonlinear systems, which offer a suitable platform to research nonlinear phenomena and dissipative solitons properties [4]. Anomalous discoveries of chaotic but local time structures have been made, such as soliton rain [5], noise-like pulse [6], and soliton explosions [7]. Additionally, stable DSs can be found in ultrafast mode-locked fiber laser systems with positive net group velocity dispersion (GVD), due to the dynamical balance between nonlinearity, dispersion, gain, and loss. They are fixed solutions in the dissipative system [8]. In other words, there is a continuous energy exchange between the DSs and environmental perturbations, along with the redistribution of energy between various parts of the pulses, resulting in a nonuniform phase across the profile of the DSs [9].

DSs formed in dissipative fiber laser systems show extremely complex dynamics and high application value [10,11]. For example, the energy and peak power of DSs are much larger than those of conventional solitons [12,13]. Stable DSs have linear phase chirp, which makes them an ideal light source for high-energy stabilized pulses, and phase-dependent optical processing [14,15]. Therefore, following theoretical analysis and experimental exploration, dissipative soliton fiber lasers have been extensively studied to improve their output performance [16–19]. The rapidly developed dispersive Fourier transform (DFT) technique soon opens new opportunities for investigating the rather complex dynamics of DSs. By utilizing dispersion, DFT maps the spectrum of an optical pulse to a temporal waveform whose intensity mimics the spectrum, allowing a photodetector to capture the real-time spectrum with a scan rate significantly beyond that of a conventional optical spectrum analyzer [20]. The transient and nonlinear dynamics are revealed soon after, including the buildup dynamics of DSs in an ultrafast fiber laser with net-normal dispersion [21], the soliton explosion, etc. [22–25]. In parallel with spectral measurements technology, a temporal magnifier technique, also known as a time-lens, was also employed to characterize the real-time temporal properties of transient DSs [26,27]. The development of the temporal analogue of a spatial lens facilitated real-time full-field characterization of transient DSs dynamics. Given the excellent works in both spectral and temporal space, another important parameter for optics, the state of polarization (SOP), has received little attention, making a full and comprehensive analysis of any vector DSs incomplete.

Recently, indirect single-shot measurements of polarization dependence have been performed based on DFT technique together with polarization beam splitters or optical filters, and solitons with complex polarization evolution processes, including polarization locking [28,29], polarization rotation [11,30], and polarization rogue waves have been identified [24,31,32]. Nevertheless, the above techniques detect the filtered polarization dynamics, either in a specific polarization state or a specific wavelength. Considering the ultrawide wavelength range for the DSs, a single-shot, wavelength-resolved polarization measurement would provide more information. The significance of such testing lies in the fact that it would reveal the genuine evolving process for the vectoral solitons: the variations for all longitudinal modes in polarization space denote phase variations of pulses within the corresponding roundtrips. The direct observation seems to be even more urgent for DSs formed within cavities with nonuniform gain across the entire wavelength, through which energy redistributes nonlinearly on the whole spectrum from roundtrip to roundtrip. The nonuniform phase across the profile of DSs can be vividly represented by the single-shot, wavelength-resolved polarization states on the Poincaré sphere. Therefore, the precise characterization of the wavelength-resolved polarization of ultrafast lasers is of great fundamental and technological significance. Nevertheless, the single-shot, wavelength-resolved polarization measurements cannot be achieved by commercial polarization analyzers, which are proposed for testing continuous wave lasers. Additionally, just recently, our group demonstrated a new technique for the single-shot measurement of wavelength-resolved polarization by combining the division-of-amplitude technique with the DFT [33]. Such a scheme is suitable for characterizing ultrafast lasers, especially for DSs with broad spectra.

In this paper, we experimentally observed the internal asymmetric evolution of DSs in polarization space. DSs are obtained by controlling the cavity structure to achieve net normal dispersion, where a saturable absorber (SA) based on a single-walled carbon nanotube is used as a mode locker. We use the division-of-amplitude method combined with DFT technique to analyze the wavelength-resolved SOPs of DSs. Wavelength-resolved polarization measurement reflects the phase evolution, which breaks through the limitations of traditional measurement methods. By adjusting the birefringence distribution in the cavity, we obtain DSs with four different spectral shapes. The nonlinear phase evolution within numerous temporal roundtrips results in the asymmetric broadening of the spectrum. We observe that the wavelength-resolved symmetry in polarization space is broken due to the phase difference among lasing wavelengths.

2. Experiment Setup

Figure 1 depicts the experimental setup, including a passively mode-locked fiber laser, a real-time spectral measurement system based on DFT, and a wavelength-resolved SOP measurement system. The ultrafast fiber laser system is configured with a net normal dispersion to ensure that it can support the generation of DSs with typical rectangular spectra. In the ring laser cavity, 11.1 m erbium-doped fiber (EDF, Nufern, EDFC-980-HP) provides optical gain with a dispersion coefficient of 15.8 ps^2/km; a 980 nm CW laser is pumped forward through a wave division multiplexer (WDM). The homemade single-walled carbon nanotubes (SWNT) film is used as SA to achieve stable mod-locking operation [34]. The low saturation power of single-walled carbon nanotubes allows our laser system to operate in the soliton state with relatively low pumping power. The polarization-independent isolator (ISO) is used to ensure unidirectional operation of the laser. A fiber-based polarization controller (PC) is inserted into the cavity to precisely adjust the net cavity birefringence. By mechanically adjusting the PC, the effective gain and filtering effects in modulating DSs are manipulated flexibly. As a result, we obtained dissipative soliton operation states of a variety of asymmetric spectra. A 90:10 optical coupler (OC) was used to extract ultrafast pulses from the laser cavity for measurement. The remaining fiber in the cavity is a 7.4 m standard single-mode fiber (SMF) with a dispersion of -22.9 ps^2/km. Therefore, the total cavity length of the fiber laser is 18.5 m and the net dispersion is 0.007 ps^2. DSs are balanced through an energy exchange with the environment in the presence of nonlinearity and dispersion. The threshold of the passively mode-locking fiber laser is 26 mW.

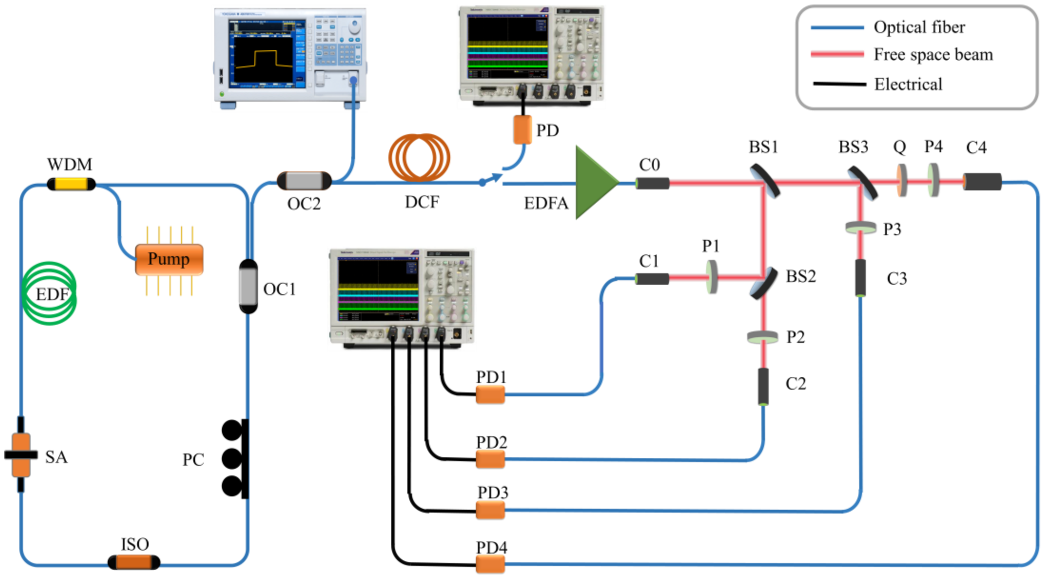

Figure 1. Schematic of the dissipative soliton fiber lasers and measurement system.

The output pulse from the fiber laser cavity is characterized by an autocorrelator (A.P.E, Pulse check USB 150), an electrical spectrum analyzer (RIGOL, DSA815), and an optical spectrum analyzer (OSA, YOKOGAWA, AQ6370D) for observing average spectrum. Meanwhile, we obtained the shot-to-shot spectra by means of the DFT system. Periodic pulses are stretched by a 2 km dispersion compensation fiber (DCF) with a dispersion of 1030 ps^2 for the frequency-to-time transformation. When a train of optical pulses enters the DCF, the spectrum of each pulse is mapped to a temporal waveform by the large GVD in the dispersive element. When neglecting higher-order dispersion terms, a linear wavelength-to-time mapping is obtained according to the relationship [20]:

$$\Delta t = |D| L \Delta\lambda \tag{1}$$

where, Δt is the time duration after mapping, D is the group delay dispersion coefficient, L is the propagation distance, and $\Delta\lambda$ is the optical spectral bandwidth of the laser pulses. Subsequently, the stretched signals are fed to an 8 GHz photodetector (PD) connected to the oscilloscope (Tektronix, DPO 71254) with a bandwidth of 20 GHz. To record wavelength-resolved, real-time SOP evolution, we combined DFT technique with division of amplitude in the spatial part [35,36]. An erbium-doped fiber amplifier (EDFA, Amonics AEDFA-23-B-FA) is used to compensate for the loss introduced by DCF and various other components. We built the spatial system through a collimator (C0); the space beam is divided into four paths with three 5:5 beam splitters (BS1-BS3). The amplitude division of four channels can be used to measure the Stokes parameter with high speed. Each path is decomposed via polarization projection through a polarizer. The fixed angles of the four polarizers (P1-P4) are 0°, 90°, 45°, and 135°, respectively. The Intersection angle between quarter-wave-plate(Q) and P4 in the fourth channel is fixed as 45°. The outputs from the four channels are received by four collimators (C1-C4). Finally, the optical signals are converted into electrical signals by four identical high-speed PDs (PD1-PD4) with a bandwidth of 8 GHz, and the final data are displayed and collected by the same oscilloscope. By calibrating the wavelength-dependent system matrix and measuring the optical intensity of the four channels, the single-shot, wavelength-resolved SOPs can be calculated as:

$$S(\lambda) = A^{-1}(\lambda)I(\lambda) \tag{2}$$

where, $S(\lambda)$ represents the wavelength-resolved Stokes vector parameters, $A^{-1}(\lambda)$ is the wavelength-dependent system matrix, and $I(\lambda)$ is the measured intensity vector from the four channels. We chose a step of 0.5 nm for the calibration of matrices. According to the devices used in our experimental facility, the minimum spectral resolution of the measurement system is about 0.2 nm, and the detection error is about 7%. More details about the wavelength-resolved SOPs measurement system can be found in Ref. [33].

3. Results

3.1. DSs with Flat Spectrum

For the mode-locked fiber laser system in Figure 1, increasing the pump power to 28 mW, DSs with a relatively flat spectrum can be obtained by appropriately adjusting the intra-cavity PC. Figure 2 shows the laser performance in this state. The measured autocorrelation trace of the output pulse is shown in Figure 2a, indicating that the pulse FWHM duration is about 11.37 ps, after fitting with a Gaussian function. The radiofrequency (RF) measurements in Figure 2b characterize the high stability of pulse intensities. The repetition rate of the fundamental frequency is ∼12.3 MHz, matching exactly with the 18.5 m cavity length. The signal-to-noise ratio at the fundamental frequency is 67 dB, indicating relatively low amplitude fluctuations. It can be found from the inset of Figure 2b that the pulse train with a bandwidth of 1 GHz has a relatively stable intensity distribution. Figure 2c shows the averaged optical spectrum measured by OSA. The typical rectangular spectrum indicates the formation of DSs under normal dispersion. The spectrum is centered at 1560.25 nm, with a spectral bandwidth of 12.5 nm. In the wavelength range from 1560 nm to 1562 nm, there is a small protuberance. Figure 2d,e plot a single shot, and consecutive spectra of the output pulses, respectively. It can be seen that the shot-to-shot spectrum at the 250th round trip (RT) is same as the OSA-measured spectrum. The consecutive spectra obtained by DFT are nearly indistinguishable within 500 RTs, verifying that the DSs have high stability.

Both averaged and single-shot spectra only recorded the intensity information of pulses. SOPs reflect the internal phase evolution of the pulses. Although the spectrum of DSs is rather flat and symmetric, the corresponding SOPs distribution in the polarization space may be rather complicated and asymmetric, as their phases across the lasing wavelengths may be nonlinearly correlated. Both averaged and single-shot spectra can only represent the scalar properties of DSs, and it is difficult to reveal the vector properties of DSs. Based on our proposed high-speed polarization measurement, the single-shot, wavelength-resolved SOPs can be measured directly. Here, the output pulses are injected into the polarization measurement system, where the temporal–spectral mapping is realized by using DFT, and the spatial configuration achieves the amplitude division of the signal. As shown in Figure 3a, the single-shot spectra of four channels are uniformly evolving without additional detail structures. Due to the specific angle of decomposition for each channel, the spectral profiles are different. According to the principle of division of amplitude, SOPs can be calculated from the intensities vector of the four channels and the calibrated Muller matrix of the measuring system [37]. We calculate SOPs in the spectral wavelength ranging from 1554 nm to 1566.5 nm with a step of 0.5 nm. The obtained normalized Stokes parameters within 500 RTs are shown on Poincaré sphere in Figure 3b. As illustrated, although slight scattering is shown in each wavelength, the comprehensive polarization distributions are rather regular. They exhibit a kind of symmetry in the polarization space. For example, the SOPs of wavelengths ranging from 1554 nm to 1560 nm are located linearly on the Poincaré sphere due to the cumulative nonlinear phase shifts for different lasering wavelengths. A similar evolutionary trajectory is shown for wavelengths ranging from 1562 nm to 1566 nm, except that the SOPs for wavelengths between 1563.5 nm and 1564 nm have relatively large spacing, which indicates sharp phase changes. Interestingly, the turning point of polarization on the Poincaré sphere occurs at 1560 nm to 1562 nm, corresponding to the protuberance on the averaged spectrum (Figure 2c). To compare the difference of SOPs for different wavelengths quantitatively, we selected three representative wavelengths within 500 consecutive RTs. As shown in Figure 3c, for wavelength at 1556 nm and 1560 nm, the Stokes parameters for consecutive RTs are rather fixed. On the contrary, the Stokes parameters fluctuate for wavelength at 1563.5 nm.

3.2. DSs with Spectrum Slanting to Red Wavelength Side

The solitons in a dissipative system are fixed localized solutions, and the distribution of DSs is indeed fixed for given parameters, but different distributions can also be obtained by adjusting these parameters. Here, we change the birefringence distribution in the cavity by adjusting PC. Nonlinear effects, dispersion, gain, and loss reach a balance again, and we obtain DSs with optical spectrum slanting to the red wavelength side. We used DFT to check the real-time optical spectra of DSs. Figure 4a demonstrates that the DSs operate in a stationary mode-locking state. The single-shot spectrum at 250 RT manifests slanting to the red wavelength side, as same as the averaged spectrum measured by OSA. As displayed in Figure 4b, an inflection point occurs at 1558.5 nm of the spectrum. At the same time, the spectral contour shows imperceptible curvature changes at 1563.5 nm. Similarly, we calculate the SOPs for the entire spectrum with a spacing of 0.5 nm. As presented in Figure 4c, the SOPs evolution trajectory located on Poincaré sphere has two obvious turning points, which correspond to curvature changes at 1558.5 nm and 1563.5 nm of the averaged spectrum. It is also found that the distance between the SOPs evolution trajectory of the blue wavelength part (1558 nm–1561 nm) is smaller than that of the red wavelength part (1563 nm–1567 nm), implying that the red wavelength part cumulates larger phase shifts than that of the blue wavelength part. Comparing with DSs with flat spectrum in the Section 3.1, the polarization trajectory for this state exhibits clear symmetry breaking in the polarization space.

3.3. DSs with Spectrum Slanting to Blue Wavelength Side

For the normally dispersed fiber cavity, we constructed strongly dissipative effects per roundtrip to reshape the pulse formation, as well as the characteristic parameters. Similarly, the effective gain and filtering effect can also be manipulated to a very different state by adjusting PC mechanically. The corresponding optical spectrum of DSs we obtained here is slanting to the blue wavelength side, and the averaged spectrum is shown in Figure 5b. The averaged spectrum ranges from 1553.5 nm to 1565.5 nm, and protuberance appears between 1559.5 nm and 1561 nm. In order to further observe the spectral evolution, 500 consecutive roundtrips' shot-to-shot spectra are measured by utilizing the DFT technique, as presented in Figure 5a. We found that even the single-spectral profile is tilted in the opposite direction; the DSs remain rather stable. However, the nonlinear phase distribution across the lasing wavelengths can be different, which can be revealed in the polarization space. According to the above procedure, SOPs for the entire spectrum are reconstructed and plotted on the Poincaré sphere in Figure 5c. Similarly to that in Figure 4c, the SOPs distribution along the wavelength for the center part are quasi-linear, while those for the blue and red wavelength sides evolve in the same directions. The distribution of SOPs depends on the internal phase of DSs. The frequency chirp is an important feature of DSs. In the conventional state, the internal phase of DSs is quasi-linearly distributed, which has been reported by Ref. [38]. Therefore, the distribution of SOPs along the wavelength of the central part is quasi-linear. However, symmetry breaking would break the quasi-linear distribution of SOPs, especially for wavelengths at the two sides. Similar turning points appear for wavelengths at 1559.5 nm and 1562.5 nm. The span ranges for the blue and red wavelength sides are also different, originating from very different phase distributions. Generally, the polarization trajectory for DSs operating in this state exhibits another shape of symmetry breaking in the polarization space.

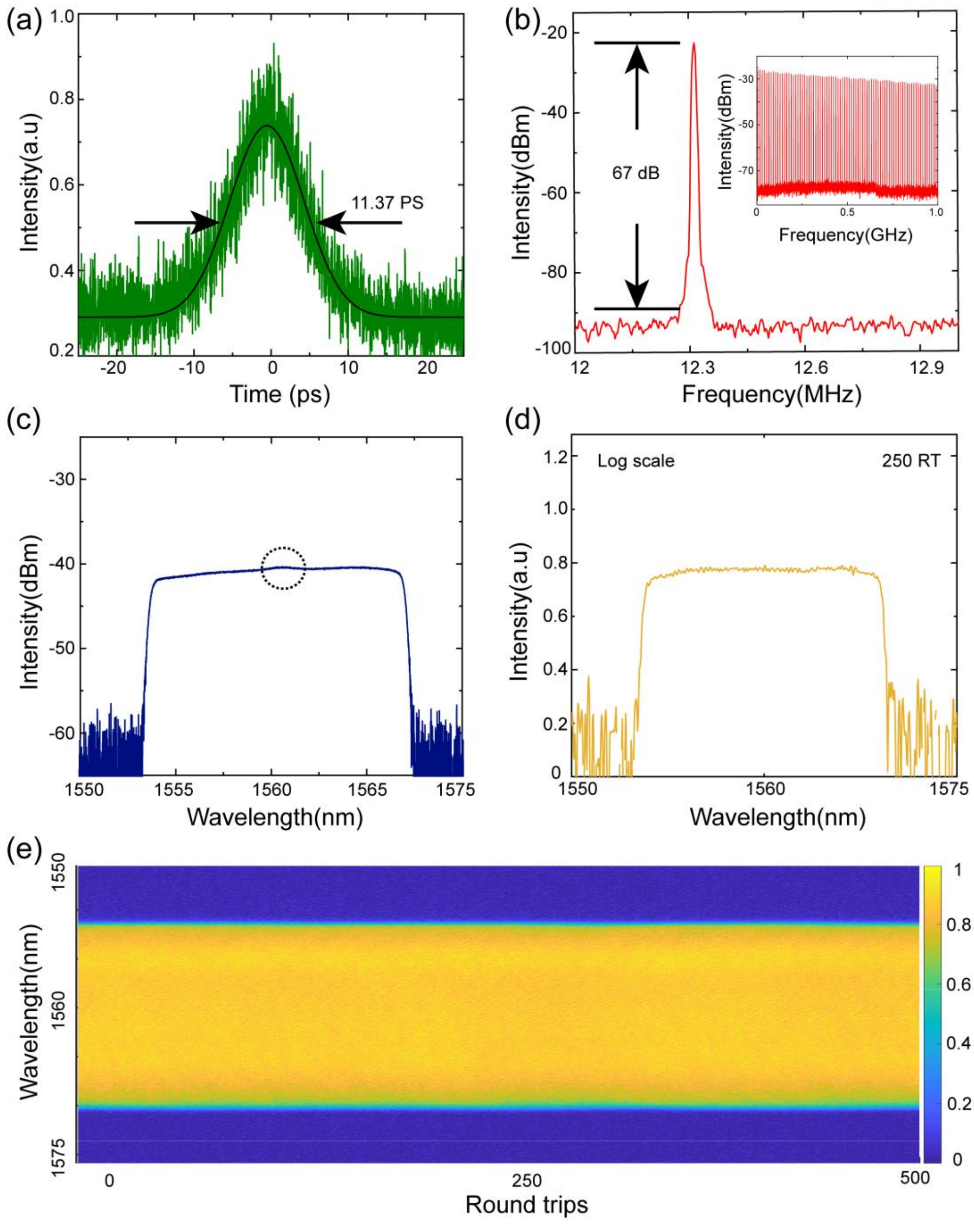

Figure 2. (**a**) Autocorrelation trace of DSs. (**b**) RF spectrum of the pulse train. (**c**) Optical spectrum of DSs measured by OSA. (**d**) single-shot spectrum at 250 RT by DFT (**e**) shot-to-shot spectral evolution by DFT.

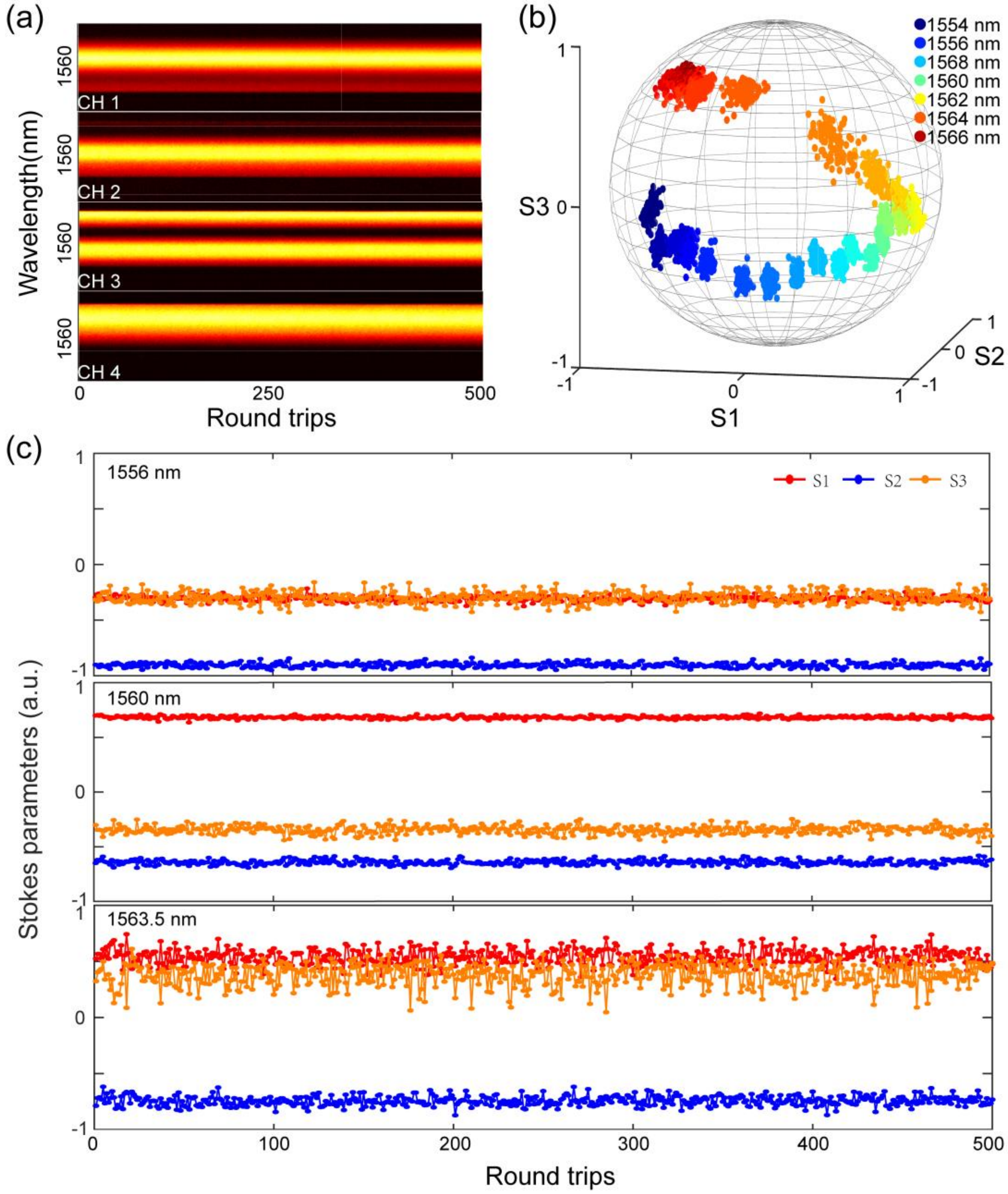

Figure 3. (**a**) Single-shot optical spectra of four channels. (**b**) Wavelength-resolved SOPs on Poincaré sphere. (**c**) RT-resolved SOPs at selected three wavelengths.

3.4. DSs with Distorted Spectrum

A more sophisticated polarization distribution can be obtained by finely adjusting the PC. A typical example of DSs with distorted spectrum is given in Figure 6. Its optical spectrum in Figure 6b exhibits nonuniform evolution, and particularly, a distinct cave shape around 1562.5 nm. However, the single-shot spectra within 500 RTs in Figure 6a indicate that the DSs operation is rather stable. One can see from the 250th RT cross-section in Figure 6a that the spectrum measured by the DFT has almost the same profile as that measured by OSA. We also map the SOPs on Poincaré sphere with a wavelength spacing of 0.5 nm, as displayed in Figure 6c. Correspondingly, from 1555 nm to 1562.5 nm, the evolutionary trajectory of SOPs on Poincaré sphere is nonuniform, with an obvious turning point at 1562.5 nm. SOPs showed scattered distributions for wavelengths ranging from 1563 nm to 1567 nm. For a quantitative investigation of the polarization features, we plotted single-shot spectra of four channels, and the reconstructed Stokes parameters of three representative wavelengths within 500 consecutive RTs in Figure 7. We can determine from Figure 7b that SOPs for a wavelength shorter than 1562.5 nm maintain a stable evolution state, while SOPs for the red wavelength sides fluctuate significantly. The reason for this can be found in Figure 7a, where single shot spectra of CH4 in the black dotted box shows fine stripe structures. Specifically, regarding the spectra in Figure 6a, it has a complex phase structure. It is possible to observe the spectral profile tilt in the opposite direction, although we did not observe the exact same spectral profile with the opposite direction during experiments. Considering the multiple parameters in the fiber laser cavity, more complex phase structures soliton pulse might appear.

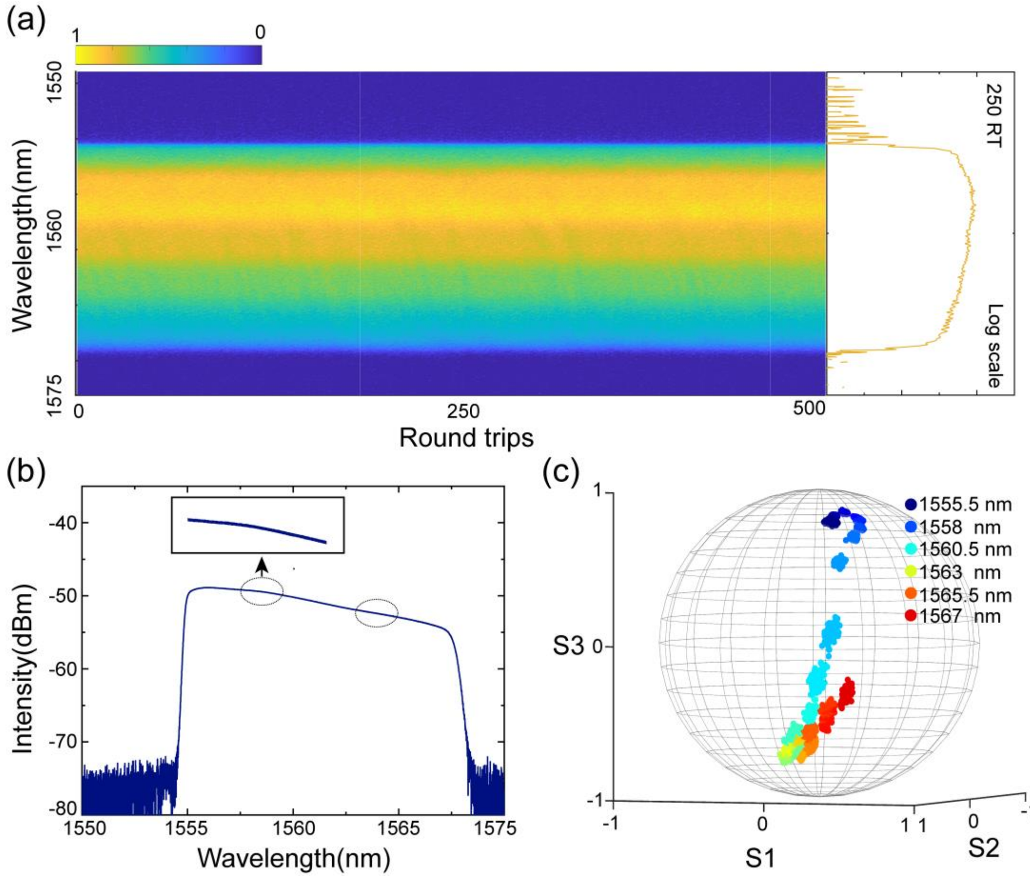

Figure 4. Spectra and SOP for DSs with spectrum slanting to red wavelength side. (**a**) Shot-to-shot spectral evolution detected by DFT. (**b**) Optical spectrum measured by OSA. (**c**) Wavelength-resolved SOPs on Poincaré sphere.

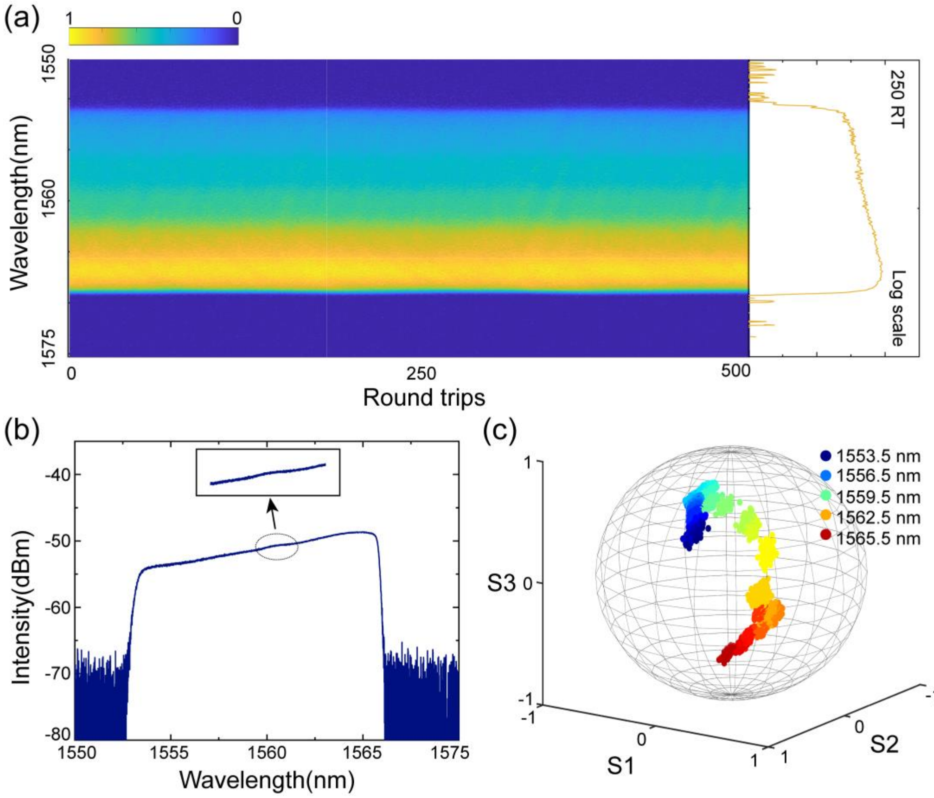

Figure 5. Spectra and SOP for DSs with spectrum slanting to blue wavelength side. (**a**) Shot-to-shot spectral evolution detected by DFT. (**b**) Optical spectrum measured by OSA. (**c**) Wavelength-resolved SOPs on Poincaré sphere.

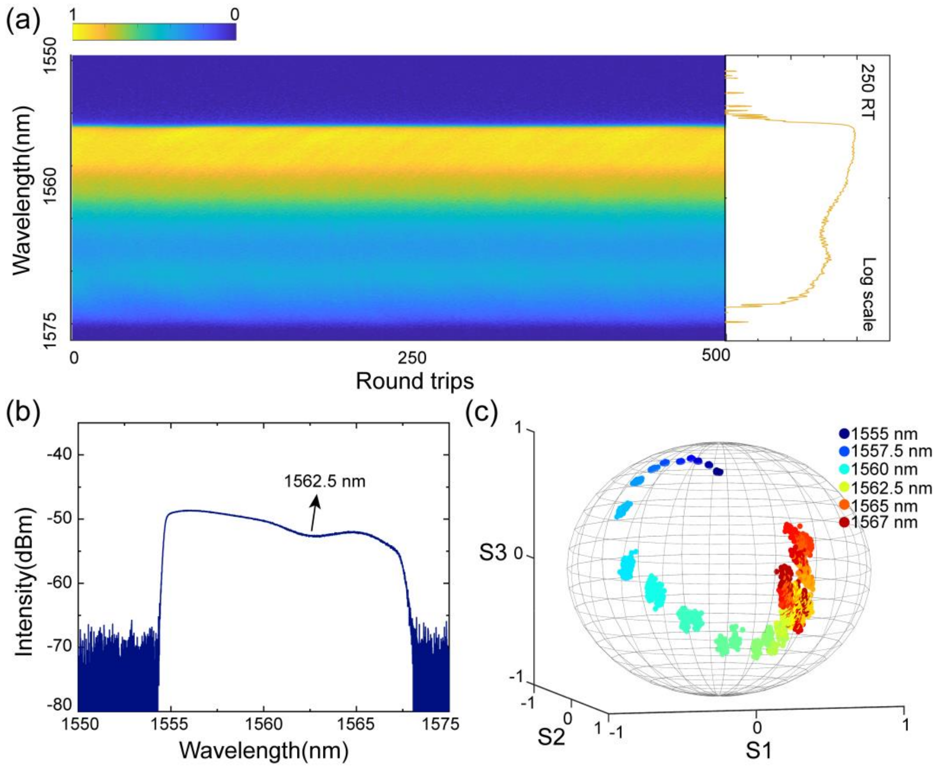

Figure 6. (**a**) Shot-to-shot spectral evolution measured by DFT. (**b**) Optical spectrum measured by OSA. (**c**) Wavelength-resolved SOPs on Poincaré sphere.

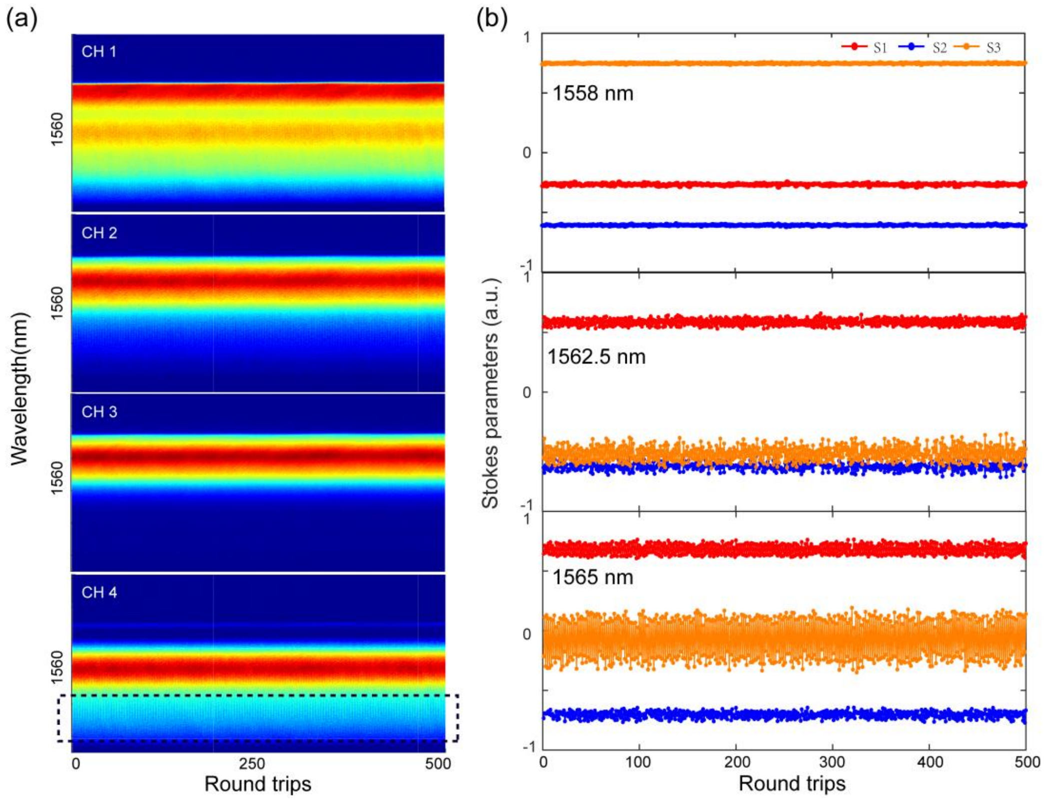

Figure 7. (**a**) Single-shot optical spectra obtained in the four channels. (**b**) RT-resolved SOPs at three selected wavelengths.

4. Discussion

At present, DSs are regarded as a kind of solution to the Ginzburg–Landau equations (CGLEs), with strong dissipations in the form of continuous energy exchange with the environment. The reallocation of energy between various parts of the solitons may prevent the formation of linear phase relations, but may build pulses with rather complex phase distributions. In essence, DSs are highly sensitive to specific parameters of the CGLEs. In our experiment, the pump intensity and the total dispersion in the cavity are fixed, and the sole adjustable parameter is PC-induced birefringence. Due to the nonuniform and polarization-dependent gain fiber we used, the effective gain and filtering effects in modulating DSs are manipulated flexibly by mechanically adjusting the PC. The DSs can still remain stable for different PC settings, through energy couplings among all longitudinal modes, while their spectra may evolve asymmetrically; namely, the red and blue wavelength sides of the spectrum broaden rather differently. Therefore, the asymmetric distribution of spectrum is the result of the combination of spectrum broadening, birefringence, and gain spectrum filtering. Further theoretical analysis is needed, with a focus on cavity parameters setting in modeling DSs based on CGLEs.

Given the direct relation between phase and polarization, the hidden asymmetry can be revealed more clearly in polarization space. Adjusting PC will not only change the linear phase but also affects the accumulation of nonlinear phases [39], resulting in the asymmetrical distribution on the Poincaré sphere. Energy flows through phase gradients, and redistribution of energy maps to a nonuniform phase profile [4]. The direct single-shot measurement of phase for transient pulses is still missing. However, we can infer the phase evolution by wavelength-resolved polarization measurements present here. It is well known that during the formation of DSs, energy flows to the two sides from the center [21,24,26]. The distribution of the SOPs on the Poincaré sphere shows that wavelengths in the two sides possess very different phases. These wavelength-dependent nonlinear phase distributions are proved by the different span ranges in the evolutionary trajectory of SOPs on the Poincaré sphere. As a result, the polarization trajectories for abnormal states of DSs exhibit complex symmetry breaking in the polarization space. The abrupt changes of phase result in the symmetry breaking in polarization space. It is therefore possible to obtain the chirp-free DSs reported in Ref. [40]. Nevertheless, it is a technical challenge to achieve this.

Despite the distribution of SOPs varying significantly for different states in part 3, the DSs pulse is very stable. Conventionally, a DS is considered to be stable once it has fixed optical spectrum, intensity, pulse width, etc. In our experiment, we found that the DSs have fixed optical spectrum, and the wavelength resolved SOP distributions over multiple roundtrips. As the SOP distribution reflects the internal phase of the soliton pulse, we can conclude that abrupt changes in the internal phase of pulse would not affect the stable operation state of DSs. Our experimental results provide important new insights into the internal dynamics of DSs, which have important implications for sound theoretical modeling and technical applications of fiber lasers.

5. Conclusions

We investigated the internal asymmetric evolution of DSs and observe the hidden asymmetry in polarization space. The single-shot, wavelength-resolved SOPs were obtained by combining the amplitude segmentation technique with the DFT. We measured four types of spectra and calculated the corresponding SOPs distributions. We observed that the trajectory of polarization evolution on the Poincaré sphere is related to the shape of DSs spectrum, which possesses nonlinear phase evolution. The physics may be attributed to the PC-induced birefringence, through which the nonuniform, polarization-dependent gain and filtering effects reshape the DSs. The polarization trajectories for abnormal profiles of DSs exhibit complex symmetry breaking in the polarization space. We believe that our results will stimulate further research of the internal dynamics of DSs, which will have great implications for improving numerical modeling and ultrafast fiber laser applications.

Author Contributions: Conceptualization and visualization, Y.L., Z.C. and L.G.; methodology, Y.L. and Q.W.; data curation and software, Q.W., A.L., Z.C. and Y.Y.; investigation and discussion, S.D., L.H., P.C. and T.Z.; writing—original draft, Y.L.; writing—review and editing, project administration and funding acquisition, L.G. and T.Z.; supervision, L.G. All authors have read and agreed to the published version of the manuscript.

Funding: This research was funded by Natural Science Foundation of China, grant number 62075021; Graduate research and innovation foundation of Chongqing, China, grant number CYB20061.

Institutional Review Board Statement: Not applicable.

Informed Consent Statement: Not applicable.

Data Availability Statement: The data that support the findings of this study are available on request from the corresponding author, L. Gao, upon reasonable request.

Conflicts of Interest: The authors declare no conflict of interest.

References

1. Arrowsmith, D.K.; Cartwright, J.H.; Lansbury, A.N.; Place, C.M. The Bogdanov map: Bifurcations, mode locking, and chaos in a dissipative system. *Int. J. Bifurc. Chaos* **1993**, *3*, 803–842. [CrossRef]
2. Ankiewicz, A.; Akhmediev, N. *Dissipative Solitons: From Optics to Biology and Medicine*; Springer: Berlin/Heidelberg, Germany, 2008.
3. Renninger, W.; Chong, A.; Wise, F. Dissipative solitons in normal-dispersion fiber lasers. *Phys. Rev. A* **2008**, *77*, 023814. [CrossRef]
4. Grelu, P.; Akhmediev, N. Dissipative solitons for mode-locked lasers. *Nat. Photonics* **2012**, *6*, 84–92. [CrossRef]
5. Chouli, S.; Grelu, P. Soliton rains in a fiber laser: An experimental study. *Phys. Rev. A* **2010**, *81*, 063829. [CrossRef]
6. Horowitz, M.; Barad, Y.; Silberberg, Y. Noiselike pulses with a broadband spectrum generated from an erbium-doped fiber laser. *Opt. Lett.* **1997**, *22*, 799–801. [CrossRef]
7. Cundiff, S.T.; Soto-Crespo, J.M.; Akhmediev, N. Experimental evidence for soliton explosions. *Phys. Rev. Lett.* **2002**, *88*, 073903. [CrossRef] [PubMed]
8. Mihalache, D.; Mazilu, D.; Lederer, F.; Leblond, H.; Malomed, B. Stability of dissipative optical solitons in the three-dimensional cubic-quintic Ginzburg-Landau equation. *Phys. Rev. A* **2007**, *75*, 033811. [CrossRef]

9. Tang, D.; Zhao, L.-M.; Zhao, B.; Liu, A. Mechanism of multisoliton formation and soliton energy quantization in passively mode-locked fiber lasers. *Phys. Rev. A* **2005**, *72*, 043816. [CrossRef]
10. Kieu, K.; Renninger, W.; Chong, A.; Wise, F. Sub-100 fs pulses at watt-level powers from a dissipative-soliton fiber laser. *Opt. Lett.* **2009**, *34*, 593–595. [CrossRef]
11. Krupa, K.; Nithyanandan, K.; Grelu, P. Vector dynamics of incoherent dissipative optical solitons. *Optica* **2017**, *4*, 1239–1244. [CrossRef]
12. Yun, L. Generation of vector dissipative and conventional solitons in large normal dispersion regime. *Opt. Express* **2017**, *25*, 18751–18759. [CrossRef] [PubMed]
13. Chen, J.-X.; Li, X.-Y.; Li, T.-J.; Zhan, Z.-Y.; Liu, M.; Li, C.; Luo, A.-P.; Zhou, P.; Wong, K.K.-Y.; Xu, W.-C. 1.7-μm dissipative soliton Tm-doped fiber laser. *Photonics Res.* **2021**, *9*, 873–878. [CrossRef]
14. Zhang, H.; Zhang, S.; Li, X.; Han, M. Optimal design of higher energy dissipative-soliton fiber lasers. *Opt. Commun.* **2015**, *335*, 212–217. [CrossRef]
15. Chi, H.; Liu, B.; Song, Y.; Hu, M.; Chai, L.; Shen, W.; Liu, X.; Wang, C. Nonlinearity optimization of dissipative-soliton fiber laser for generation of pulses with 350 kW peak power. *High Power Laser Sci. Eng.* **2018**, *2*, 98–102. [CrossRef]
16. Moores, J.D. On the Ginzburg-Landau laser mode-locking model with fifth-order saturable absorber term. *Opt. Commun.* **1993**, *96*, 65–70. [CrossRef]
17. Cabasse, A.; Ortaç, B.; Martel, G.; Hideur, A.; Limpert, J. Dissipative solitons in a passively mode-locked Er-doped fiber with strong normal dispersion. *Opt. Express* **2008**, *16*, 19322–19329. [CrossRef]
18. Liu, X. Hysteresis phenomena and multipulse formation of a dissipative system in a passively mode-locked fiber laser. *Phys. Rev. A* **2010**, *81*, 023811. [CrossRef]
19. Yun, L.; Liu, X.; Mao, D. Observation of dual-wavelength dissipative solitons in a figure-eight erbium-doped fiber laser. *Opt. Express* **2012**, *20*, 20992–20997. [CrossRef]
20. Goda, K.; Jalali, B. Dispersive Fourier transformation for fast continuous single-shot measurements. *Nat. Photonics* **2013**, *7*, 102–112. [CrossRef]
21. Chen, H.-J.; Liu, M.; Yao, J.; Hu, S.; He, J.-B.; Luo, A.-P.; Xu, W.-C.; Luo, Z.-C. Buildup dynamics of dissipative soliton in an ultrafast fiber laser with net-normal dispersion. *Opt. Express* **2018**, *26*, 2972–2982. [CrossRef]
22. Peng, J.; Zeng, H. Soliton collision induced explosions in a mode-locked fibre laser. *Commun. Phys.* **2019**, *2*, 34. [CrossRef]
23. Runge, A.F.; Broderick, N.G.; Erkintalo, M. Observation of soliton explosions in a passively mode-locked fiber laser. *Optica* **2015**, *2*, 36–39. [CrossRef]
24. Gao, L.; Cao, Y.; Wabnitz, S.; Ran, H.; Kong, L.; Li, Y.; Huang, W.; Huang, L.; Feng, D.; Zhu, T. Polarization evolution dynamics of dissipative soliton fiber lasers. *Photonics Res.* **2019**, *7*, 1331–1339. [CrossRef]
25. Yu, Y.; Luo, Z.-C.; Kang, J.; Wong, K.K. Mutually ignited soliton explosions in a fiber laser. *Opt. Lett.* **2018**, *43*, 4132–4135. [CrossRef]
26. Suret, P.; Koussaifi, R.E.; Tikan, A.; Evain, C.; Randoux, S.; Szwaj, C.; Bielawski, S. Single-shot observation of optical rogue waves in integrable turbulence using time microscopy. *Nat. Commun.* **2016**, *7*, 13136. [CrossRef] [PubMed]
27. Zhang, Y.; Cui, Y.; Huang, L.; Tong, L.; Liu, X. Full-field real-time characterization of creeping solitons dynamics in a mode-locked fiber laser. *Opt. Lett.* **2020**, *45*, 6246–6249. [CrossRef]
28. Tang, D.; Zhang, H.; Zhao, L.; Wu, X. Observation of high-order polarization-locked vector solitons in a fiber laser. *Phys. Rev. Lett.* **2008**, *101*, 153904. [CrossRef]
29. Mou, C.; Sergeyev, S.; Rozhin, A.; Turistyn, S. All-fiber polarization locked vector soliton laser using carbon nanotubes. *Opt. Lett.* **2011**, *36*, 3831–3833. [CrossRef]
30. Liu, M.; Luo, A.-P.; Luo, Z.-C.; Xu, W.-C. Dynamic trapping of a polarization rotation vector soliton in a fiber laser. *Opt. Lett.* **2017**, *42*, 330–333. [CrossRef]
31. Gao, L.; Kong, L.; Cao, Y.; Wabnitz, S.; Ran, H.; Li, Y.; Huang, W.; Huang, L.; Liu, M.; Zhu, T. Optical polarization rogue waves from supercontinuum generation in zero dispersion fiber pumped by dissipative soliton. *Opt. Express* **2019**, *27*, 23830–23838. [CrossRef] [PubMed]
32. Gao, L.; Wu, Q.; Cao, Y.; Wabnitz, S.; Zhu, T. Optical polarization rogue waves and their identifications. *J. Phys. Photonics* **2020**, *2*, 032004. [CrossRef]
33. Wu, Q.; Gao, L.; Cao, Y.; Wabnitz, S.; Chang, Z.; Liu, A.; Huang, J.; Huang, L.; Zhu, T. Single-shot measurement of wavelength-resolved state of polarization dynamics in ultrafast lasers using dispersed division-of-amplitude. *Photonics Res.* **2023**, *11*, 35–43. [CrossRef]
34. Li, Y.; Gao, L.; Zhu, T.; Cao, Y.; Liu, M.; Qu, D.; Qiu, F.; Huang, X. Graphene-assisted all-fiber optical-controllable laser. *IEEE J. Sel. Top. Quantum Electron.* **2017**, *24*, 0901709. [CrossRef]
35. Azzam, R. Division-of-amplitude photopolarimeter (DOAP) for the simultaneous measurement of all four Stokes parameters of light. *Opt. Acta Int. J. Opt.* **1982**, *29*, 685–689. [CrossRef]
36. Azzam, R. Beam-splitters for the division-of-amplitude photopolarimeter. *Opt. Acta Int. J. Opt.* **1985**, *32*, 1407–1412. [CrossRef]
37. Krishnan, S. Calibration, properties, and applications of the division-of-amplitude photopolarimeter at 632.8 and 1523 nm. *JOSA A* **1992**, *9*, 1615–1622. [CrossRef]

38. Kelleher, E.J.R.; Travers, J.C.; Ippen, E.P.; Sun, Z.; Ferrari, A.C.; Popov, S.V.; Taylor, J.R. Generation and direct measurement of giant chirp in a passively mode-locked laser. *Opt. Lett.* **2009**, *34*, 3526–3528. [CrossRef]
39. Du, Y.; Xu, Z.; Shu, X. Spatio-spectral dynamics of the pulsating dissipative solitons in a normal-dispersion fiber laser. *Opt. Lett.* **2018**, *43*, 3602–3605. [CrossRef] [PubMed]
40. Mao, D.; He, Z.; Gao, Q.; Zeng, C.; Yun, L.; Du, Y.; Lu, H.; Sun, Z.; Zhao, J. Birefringence-managed normal-dispersion fiber laser delivering energy-tunable chirp-free solitons. *Ultrafast Sci.* **2022**, *2022*, 9760631. [CrossRef]